TITLE:
Studies on the Quasi-Stationary Rossby Wave Trapped in the Westerly Jet in the Northern Hemisphere Summer(Dissertation_全文)

AUTHOR(S):
Terao, Toru

CITATION:
Terao, Toru. Studies on the Quasi-Stationary Rossby Wave Trapped in the Westerly Jet in the Northern Hemisphere Summer. 京都大学, 1998, 博士(理学)

ISSUE DATE:
1998-03-23

URL:
https://doi.org/10.11501/3135300

RIGHT:

京都大学学術情報リポジトリ
KURENAI 紅
Kyoto University Research Information Repository

主論文

Studies on the Quasi-Stationary Rossby Wave Trapped in the Westerly Jet in the Northern Hemisphere Summer

By Toru Terao

Abstract

The quasi-stationary Rossby wave trapped in the westerly jet (TQS-Rossby wave) is investigated from a viewpoint of the extratropical intraseasonal variations for the northern hemisphere summer.

Several essential aspects of the TQS-Rossby wave are newly discussed and confirmed. Over the Eurasian Continent in summer, the TQS-Rossby wave-like disturbance is the most prominent factor of intraseasonal variations. The case study for the 1983 summer shows that the TQS-Rossby wave of 30-45-day time scales plays an important role in regulating the intraseasonal variation of the Asian summer monsoon circulation. The upper tropospheric temperature of the Tibetan High decreases when the TQS-Rossby wave transports sensible heat northward. The zonal wavenumber and the intensity of such TQS-Rossby waves have rather clear dependency on the frequency. This is shown clearly by space-time spectral analysis and is interpreted by the β-channel model.

The original analysis tools proposed are successfully used. The ray-path analysis for the Rossby wave is extended. Not only temporally but also zonally appropriate smoothed basic flow is used instead of basic flows such as climatological or monthly mean flows smoothed only in time space. The solutions of step-like zonally symmetric basic state is examined in the β-channel model, which clearly explains the dynamical aspect of the TQS-Rossby waves. The intraseasonal variation of the Asian summer monsoon circulation is associated with the accumulation of the high potential temperature air mass transported into the upper troposphere around the Tibetan High. This accumulation is highly remarkable in the general circulations in the northern hemisphere summer.

1 Introduction

The *intraseasonal variation* is the variation of the atmosphere on time scales longer than the synoptic variations and shorter than the seasonal march. The time scale of the intraseasonal variation is considered to be self-organized in the atmosphere itself or through the interactions among the atmosphere, ocean, land surface and so on without the external forcings. Increasing the knowledge of the intraseasonal variations should extend the possibility of the long-range weather forecasts. Thus, the research on the intraseasonal variation is one of the most interesting subjects of the atmospheric sciences.

Various time scales of intraseasonal variations have been found in the atmosphere. The 30-60-day oscillation of tropical convection is one of the prominent intraseasonal variations (Madden and Julian, 1971, 1972; Lorenc, 1984). Some researchers pointed out that such intraseasonal variations are also seen in the extratropics (e.g. Krishnamurti and Gadgil, 1985). Subsequently, many researches which intend to understand the extratropical intraseasonal variations in the context of the influence of the tropical 30-60-day oscillation have found evidences indicating that the some extratropical intraseasonal variations can be explained by the Rossby wave induced by the variations of tropical convective activity (Lau and Phillips, 1986; Nitta, 1987). However, the extratropical intraseasonal variations are not always caused by the tropical intraseasonal variations. For example, Knutson and Weickmann (1987) showed that the extratropical intraseasonal variations highly correlated with the tropical 30-60-day oscillation are seldom seen in northern hemisphere summer. Simmons et al. (1983) and Tsuyuki and Kurihara (1989) emphasized that the characteristics of the extratropical circulation itself control significantly its response to the tropical forcings. These results show that the extratropical intraseasonal variations are not explained only by the influence of the tropics. Therefore, the intraseasonal variations peculiar to the extratropics should be investigated more.

Among such intraseasonal variations, the quasi-stationary Rossby wave trapped in the westerly jet is fairly important one. Recently, the waves with wavenumber 5-7 trapped in the subtropical jet on 10-30-day time scales are investigated by many researchers for northern hemisphere (Blackmon et al., 1984; Lanzante, 1990; Kiladis and Weickmann, 1992; Hsu and Lin, 1992; Shapiro and Goldenberg, 1993 for the winter, and Terao, 1995; Ambrizzi et al., 1995 for the summer), and for southern hemisphere (Berbery et al., 1992 for both of the winter and the summer). Hoskins and Ambrizzi (1993) and Yang and Hoskins (1996) have shown that these intraseasonal variations can be classified as the Rossby wave trapped in the westerly jet with slow zonal phase velocity, using the diagnostic analysis based on the ray-path theory which is called *ray-path analysis*, hereafter. In this thesis, the Rossby waves with slow zonal phase velocities (smaller than 5ms^{-1}) are referred to as *QS-Rossby waves*. And the QS-Rossby waves trapped in the westerly jet are abbreviated to *TQS-Rossby waves* (Trapped QS-Rossby waves). It has been shown that the TQS-Rossby wave is one of the most major classes of intraseasonal variations in the extratropics at least on 10-30-day time scales.

However, there remains many unknown aspects of TQS-Rossby wave. First, the researches on the relations to the other systems in the atmospheric circulation have just be-

gun. For example, Nakamura (1994) showed that the TQS-Rossby wave plays an important role in some blocking formation events. However, there are many subjects to be discussed further such as the interactions with the tropical circulations, the monsoons, the baroclinic waves and so on. Second, there are many problems on the basic properties of the TQS-Rossby wave yet. While many data analysis (Blackmon et al., 1984; Hsu and Lin, 1992; Terao, 1995; Ambrizzi et al., 1995) have shown that the TQS-Rossby wave is evident on about 10-30-day time scales, the reason is not clear. Yang and Hoskins (1996) showed that the zonal wavenumber of TQS-Rossby wave in the numerical model varies as the frequency changes. However, no data analysis investigated the relationships between the frequency and the wavenumber comprehensively. Third, the ray-path analysis which has been used to investigate the dynamics of the TQS-Rossby waves is based on the WKBJ approximation which is violated around the westerly jets, since the basic flows around there vary steeply in the meridional direction. The researches without the WKBJ assumption should be done and compared with the results obtained from the ray-path analysis. This thesis intends to solve some of these unknowns by investigating the properties of the TQS-Rossby wave.

The first purpose of this thesis is to investigate the role of the TQS-Rossby wave from a viewpoint of the relations with the Asian summer monsoon circulation. The Asian summer monsoon is an especially interesting region to investigate the tropical-extratropical interactions on the intraseasonal time scales. In this region, the Asian summer monsoon convection which is the major tropospheric heat source in northern summer penetrate northward beyond 30°N, just south of the subtropical jet (Johnson, 1992). Furthermore, it has been confirmed that the variations of this convective activity contain 10-20-day (Murakami, 1976) and 30-60-day (Yasunari, 1979) variations.

However, the relationships between Asian summer monsoon circulations and extratropical circulations on intraseasonal time scales have not been addressed clearly yet. Kuma (1985) emphasized the possibility of the influence of the thermal forcing by the variations in the Asian summer monsoon convection on the extratropical circulations through the excitation of the Rossby waves. Yasunari (1986) examined the correlations between the activity of the Indian summer monsoon convection and lower tropospheric extratropical circulations. He showed that the lower tropospheric geopotential height tends to decrease (increase) east (west) of the Tibetan Plateau with the northward shift of relatively active Indian summer monsoon convection region. However, the relationships between the extratropical circulations such as the TQS-Rossby wave and the Asian summer monsoon convection are not fully investigated especially in the upper troposphere.

The importance of the interactions between the Asian summer monsoon circulation and the extratropical disturbances has been pointed out from another point of view. Chen (1995) and Dunkerton (1995) showed that the Asian and Mexican summer monsoon plays a significant role in the stratosphere-troposphere (S/T) mass exchange. Dunkerton (1995) discussed that the S/T exchange may occur with the Rossby wave breaking on the critical latitude where the zonal phase speeds of the waves are equal to the zonal wind velocity component of the basic state. Actually, from the data analysis of the real atmosphere, the TQS-Rossby wave-like systematic intraseasonal variations are surely seen just north of the Tibetan Plateau in the northern summer (Terao, 1995; Ambrizzi et al., 1995). It suggests

that there is interaction between the TQS-Rossby wave and the Tibetan High through the wave breaking.

The second purpose is to study the general aspects of the TQS-Rossby wave more systematically. As a tool without the WKBJ assumption, the β-channel model with the zonally symmetric step-like basic state is developed (Appendix C) after Yanai and Nitta (1968). On the other hand, the space-time spectral analysis is applied to the data to extract the basic properties of the TQS-Rossby wave. Using these theoretical and analytical methods, the following questions which are relevant to the basic properties of the TQS-Rossby wave are discussed.

Q1: Dominant time scales of the TQS-Rossby waves It has been emphasized the importance of 10-30-day periods in the literature (Blackmon et al., 1984; Hsu and Lin, 1992). However, the reason have not been clarified yet.

Q2: Dominant zonal wavenumber and its dependency on the frequency The zonal wavenumber dependency on the frequency should be clarified systematically. Yang and Hoskins (1996) examined the dependency of the wavenumber of the TQS-Rossby waves on the frequency for the waves calculated in the barotropic numerical prediction model on a sphere. This result is also interpreted in the context of the ray-path analysis. However, no data analysis have shown these dependencies yet.

Q3: Strength of trapping The observations, as a whole, have shown that the eastward-propagating TQS-Rossby waves are stronger than the westward-propagating waves (Berbery et al., 1992; Hsu and Lin, 1992). The ray-path analysis also have shown that the ray-paths for the eastward-propagating TQS-Rossby waves tend to more strongly confined in the westerly jets than westward-propagating waves (Yang and Hoskins, 1996). This point should be confirmed comprehensively by the space-time spectrum analysis.

On these considerations, this thesis is organized as follows. In section 2, the properties of the intraseasonal variations over the Eurasian Continent are investigated. It is also shown that the fairly evident TQS-Rossby-wave like 30-45-day intraseasonal variation is seen in 1983 summer. By the case study for that year, it is examined whether the waveguide for the QS-Rossby waves is formed along the westerly jet or not using an extended ray-path analysis method (Appendix B.2). In section 3, the heat and mass transports on the 355K isentropic surface are examined about the 1983 summer. In section 2, the systematic zonal wavenumber-frequency and wave intensity-frequency relationships are obtained for the disturbances in the subtropical jet over the Eurasian Continent in summer. Section 4 is devoted to the elucidation of the mechanism which leads these relationships. Section 5 is concluding remarks. The equations on which this thesis is based on are derived in Appendix A. The traditional ray-path theory and its extension are defined in Appendix B. The method to solve the β-channel model used in section 4 is in Appendix C.

Refer to Terao (1998a) for more detailed discussion about section 2. See Terao (1998a) for more details of section 3.1. The results of section 3.2, 3.3 and 3.4 are mainly based on Terao (1998b). More detailed discussions for section 4 are given in Terao (1998c).

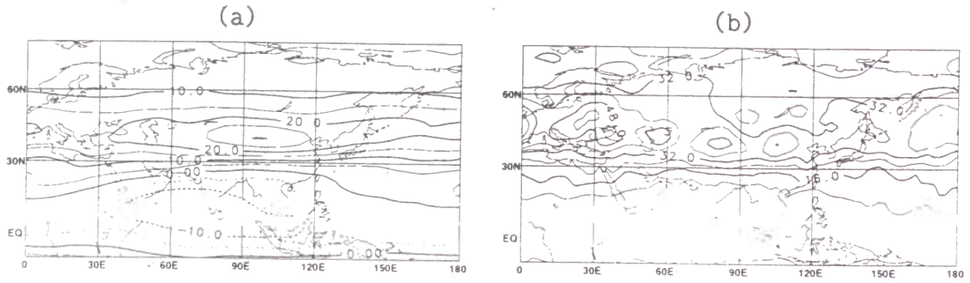

Fig. 1. The climatological summer (from June to September) mean of (a)zonal wind velocity and (b)variance of 15-60-day band-pass filtered meridional wind velocity at 200hPa. Contour intervals are $5ms^{-1}$ for (a), and $8m^2s^{-2}$ for (b).

Throughout this thesis, the ECMWF/WMO initialized analysis and the ECMWF/TOGA non initialized analysis are used for periods between 1980 and 1988 and between 1989 and 1993, respectively. Lanczos filters(Duchon, 1979) are applied to extract time series of various time scales. For the ray-path analysis and the β-channel model, the data at 300hPa are used following Grose and Hoskins (1979) which showed that the motions of real atmosphere are well modeled by barotropic atmosphere at 300hPa.

2 Properties of the intraseasonal variations over the Eurasian Continent in northern hemisphere summer

In this section, general aspects of intraseasonal variations over the Eurasian Continent in the northern summer are investigated.

2.1 The climatological spatial distribution of the intraseasonal variations

The spatial distribution of the intraseasonal variation is shown in Fig.1. From this figure, it is found that the activity of intraseasonal variations is high over some regions at intervals embedded in the zonally elongated region along 40-45°N which corresponds to the subtropical jet. The disturbances are most prominently seen at 200hPa.

2.2 The structure of the intraseasonal variation along the subtropical jet in the zonal wavenumber-frequency domain

In order to find dominant frequency bands, the power spectral densities are calculated using FFT method for daily departures of 200hPa meridional wind velocity from their climatological daily means for all grid points over the domain along the subtropical jet from June to September (see Fig.3 of Terao (1998a)). This shows that the intraseasonal variation on 30-45-day time scales is the most prominent intraseasonal variations.

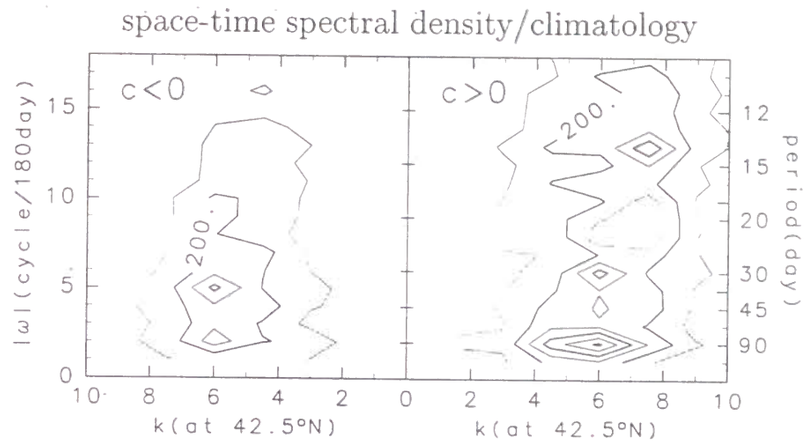

Fig. 2. The space-time power spectral density of meridional wind velocity at 200hPa in summer for average over 14 years from 1980 to 1993 along 40-45°N latitude circle from 30°W to 150°W. The horizontal axis shows zonal wavenumber. The vertical axis shows the frequency in cycle par 180-day and the period in day. While the left half shows the westward-propagating mode, the right half shows the eastward. Contour interval is $100m^2s^{-2}$day-degree.

The basic structure of the intraseasonal disturbance in zonal wavenumber-frequency domain is expressed by the space-time power spectral density (Hayashi, 1971) for 200hPa meridional wind along the subtropical jet over the Eurasian Continent (Fig.2). It shows that systematic relationships are seen among the zonal wavenumber, strength of power, and the frequency. While the wavenumber and the strength of their spectral peaks are almost the same at lower frequency range, as the frequency increases, wavenumber of eastward-(westward-) propagating mode increases (decreases) and the strength of the power of the westward-propagating mode becomes less evident than eastward-propagating one. Another prominent feature of the space-time spectral densities is the narrow range of the zonal wavenumbers, showing that the variation along the subtropical jet is characterized by its typical zonal wavelength more distinctly than by its typical frequency (period).

Furthermore, Fig.2 shows that the variation contains phenomena in remarkably longer time scales than those which have already been pointed out by Blackmon et al. (1984), Hsu and Lin (1992), Kiladis and Weickmann(1992) and Berbery et al. (1992), who have investigated variations mainly in 10-30-day band. The properties of variations on time scales longer than 30-day up to 90-day are also suggested to be important at least over Eurasian Continent. The properties of these variations are similar to those of TQS-Rossby waves

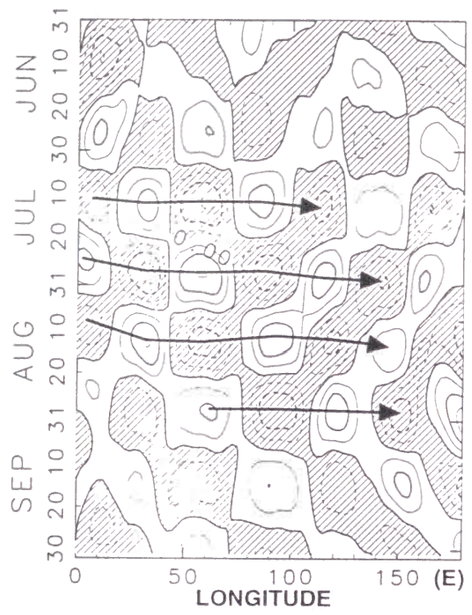

Fig. 3. Longitude-time cross sections along 40-45°N for the 25-60-day band-pass filtered meridional wind at 200hPa in 1983. Contour interval is 4ms^{-1}. Negative areas are hatched. See the text for the explanation for arrows.

which have already been described by many researchers.

2.3 The representative 30-45-day variation in 1983 summer

The year-to-year variation of the power spectral density in summer for 36-day period (Fig.3 (b) of Terao (1998a)) shows that the representative 30-45-day variation is found in 1983 summer. The 30-45-day variation along the subtropical jet in 1983 is analyzed here in detail.

The basic space-time structure of the 30-45-day disturbance in 1983 is shown in the longitude-time cross section along 40-45°N for the 25-60-day anomaly in meridional wind at 200hPa (Fig.3). It shows evident standing wave pattern with a 32-day period and 52° longitudinal wavelength. The solid lines with arrows, which connect peaks in meridional wind anomaly, show slightly downward trends. This indicates the eastward kinetic energy propagation. The pattern of 25-60-day anomalies in temperature at 300hPa in the longitude-time cross section is similar to that of meridional wind at 200hPa (Fig.3) except that the peaks are shifted about a quarter-wavelength eastward (figures are not shown). This implies that the vertical structure of disturbance is nearly barotropic.

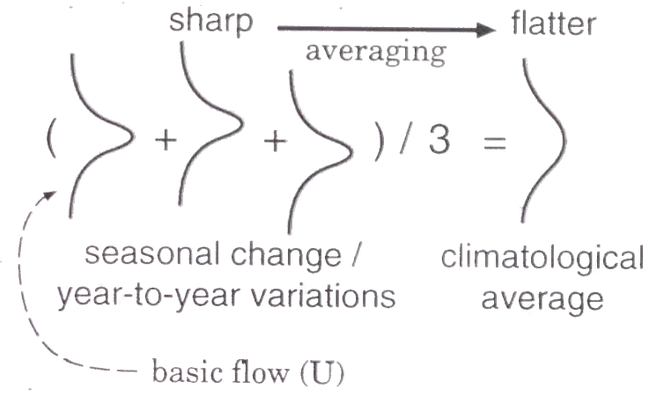

Fig. 4. A schematic diagram which shows the reason why the meridional profile of the climatologically averaged zonal flow get flatter. See text for more informations.

2.4 The extended ray-path analysis for the subtropical jet in 1983 summer over the Eurasian Continent

Here, it is examined whether the basic flow along the subtropical jet in 1983 forms the waveguide for the QS-Rossby waves or not. The ray-path analysis for the barotropic Rossby wave which is summarized in Appendix B is used. The most important variable is κ (7). For more detailed discussion, see section 5.1 of Terao (1998a)

It should be noted that the climatological basic flows defined in various way don't form the robust waveguide along the subtropical jet just north of the Tibetan Plateau. The reason is inferred as follows. As is schematically shown in Fig.4, if ever the climatologically averaged basic flow is made by averaging of many *sharp* profiles of basic flows, the profile of the resulting climatological average should get rather *flat*. Since the meridional profile of κ should also becomes flatter, the waveguide of the climatological average must be ambiguous.

As is discussed in Appendix B.2 and section 5.2 of Terao (1998a), the individual wavepacket 'feels' the basic flow in the area with certain temporal and zonal extent. Therefore, in this study, not only temporally but also zonally smoothed zonal wind is used as the basic flow. The analysis using this method enables us to examine the behavior of the individual wavepacket. This method is applied to the 30-45-day disturbance along the subtropical jet in 1983 summer.

In order to examine the properties of the basic state 'felt' by the disturbance, the 60-day low-pass filter and zonal moving average over 50°, which approximately corresponds to the wavelength of the disturbance (Fig.3), are used. The results are shown in Fig.5 by the κ distributions. Since the wavenumber of the 30-45-day variations is about 7 ($\simeq 360°/52°$), the waveguide for them is the region $\kappa > 7$ sandwiched by northern and southern smaller κ

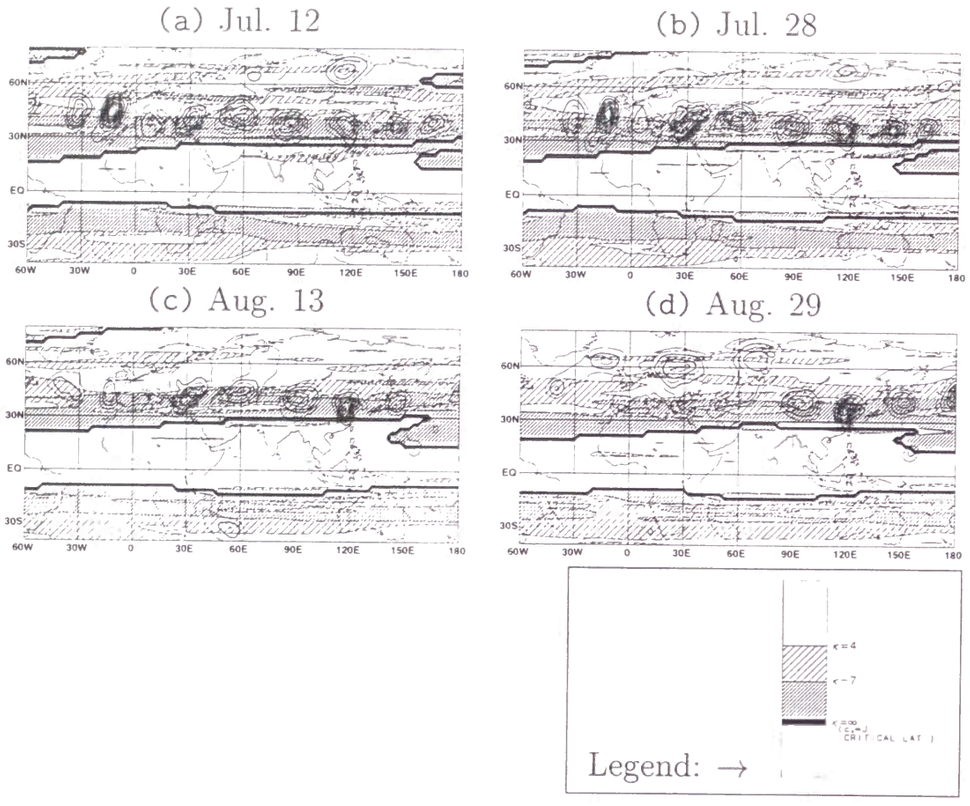

Fig. 5. The distributions of κ for the 30-45-day disturbance in the subtropical jet on four days when the TQS-Rossby wave-like disturbances are enhanced over the Eurasian Continent. The contour shows the square of the 25-60-day band-pass filtered meridional wind velocity. Its contour interval is $25\mathrm{ms}^{-1}$. See legend for the tone levels.

(< 7) regions.

On July 12 (Fig.5(a)), for instance, the following regions along the subtropical jet flowing at around 40°N are judged as waveguides.

- Over the Atlantic Ocean, from west of 60°W to 15°W. This $\kappa > 7$ region is bounded by $\kappa < 7$ regions at both of the north and south sides.
- A short waveguide near the Black Sea at around 30°E.
- Another short waveguide to the northwest of the Indian subcontinent, from 45°E to 85°E.
- A long waveguide which covers the area over the north of the Tibetan Plateau, the east of the China, the Japan Islands and the western North Pacific from 85°E to 170°E. It should be noted that a narrow but well defined $\kappa < 7$ region is recognized along 30°N from 60°E to 150°E.

Although some gaps of the waveguide can be pointed out, roughly speaking, a long waveguide extends all over the plotted domain on July 12.

On all the plotted days, largely, propagation patterns of the observed disturbances in 1983 can be explained by the extended ray-path analysis for the Rossby wave. This waveguide is separated from the critical latitude south of 30°N by a narrow region where $\kappa < 7$.

3 The heat and mass transport in the northern periphery of the Tibetan High associated with the TQS-Rossby wave along the subtropical jet in summer 1983

In this section, the case study of 1983 summer is further developed. The relationships between the Asian summer monsoon circulation and the TQS-Rossby wave over the Eurasian Continent in 1983 are investigated with the special attention to the northward heat and mass transport in the northern periphery of the Tibetan High.

3.1 Some characteristics of the TQS-Rossby wave in 1983 associated with the meridional irreversible mass and heat exchange

Following the discussion by Dunkerton (1995), the behavior of the TQS-Rossby wave near the critical latitude is focused. As is discussed by him, the wave breaking process must play intrinsic role in irreversible meridional mass and heat exchange. Figure 6(a) shows the upper tropospheric circulations over the Eurasian Continent and the western North Pacific on July 28, when the TQS-Rossby wave is intensified. It is shown that the shape of the northern part of the Tibetan High (hatched region) is strongly distorted by the TQS-Rossby wave propagating along the subtropical jet, suggesting the strong interaction between them. The

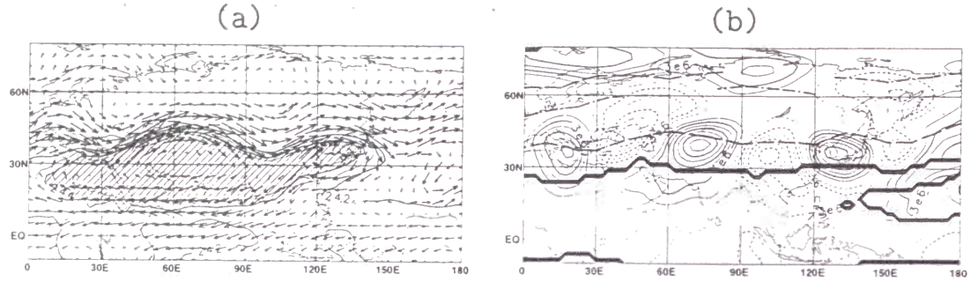

Fig. 6. (a)The 25-day low-pass filtered wind velocity vector at 200hPa and temperature at 300hPa, and (b)the 25-60-day band-pass filtered streamfunction at 200hPa on July 28, 1983. In (a), The arrow length of a grid interval gives the wind speed of about 14ms^{-1}. Contour interval is 1K, and contours less than 242K are not shown. Areas of temperatures higher than 244K are hatched. In (b), the thick dashed and dot-dashed lines indicate the axis of the strong and weak zone of the 60-day low-pass filtered zonal wind velocity, respectively. Thick solid line indicates the critical latitude where $U = 0$. Contour interval is 2×10^6m^{2}s^{-1}. Negative contours are dashed. Zero contour is ignored.

25-60-day band-pass filtered wind field and its relation to the 60-day low-pass filtered zonal wind on July 28 are shown in Fig.6(b). The southernmost part of the TQS-Rossby wave crosses the critical latitude for the stationary wave indicated by thick solid line especially to the east of 60°E. It proposes that the nonlinear processes such as breaking of the TQS-Rossby wave can occur at the critical latitude. It should be noted that this critical latitude corresponds to the center of the Tibetan High.

In section 2.3, it was noted that the TQS-Rossby wave along the subtropical jet is nearly barotropic. However, the completely barotropic disturbance can not transport heat meridionally. Therefore, the vertical phase tilt of the disturbance is investigated carefully here. The vertical phase structure of the TQS-Rossby wave along the subtropical jet (40-45°N) over the Eurasian Continent in 1983 is statistically shown in Fig.7. The complete definition of the value plotted in this figure is given in section 4.3 of Terao (1998a). The wave is nearly barotropic. However, it slightly tilts westward especially to the west of the center of wavepacket, implying the northward eddy heat transport by the TQS-Rossby wave. It also indicates the energy conversion from the available potential energy into the kinetic energy of the disturbances (Ambrizzi and Hoskins, 1997).

3.2 The thermodynamic structure and its intraseasonal variations of the upper troposphere in the Tibetan High in 1983 summer

The 8-day low-pass filtered potential temperature at 200hPa along 20-40°N from June to September in 1983 is shown in Fig.8. The temperature over 30-120°E considerably increases

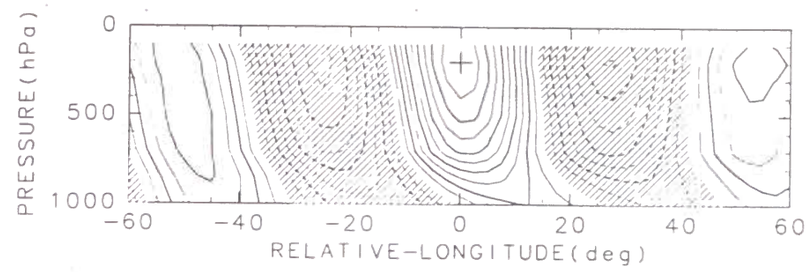

Fig. 7. The statistical vertical structure of the longitude-pressure cross sections of 25-60-day anomaly in meridional wind along 40-45°N for 1983 summer. See text for detailed explanations. Contour interval is 0.1. Zero contour is not shown. Negative areas are hatched.

at late June and decreases in late August.

Evident intraseasonal temperature variations are seen in the Tibetan High in 1983 northern summer. From the 8-day low-pass filtered potential temperature averaged over 20-40°N and 30-120°E (Fig.8(b)), three major warming events are seen (marked by ○). The intervals between these events are about 20-30 days which is somewhat shorter than the time scales of the tropical Madden-Julian oscillations (Madden and Julian, 1994). Major cooling events are found on July 13, August 4 and 30 (marked by ×).

The latitude-pressure cross sections for the 8-day low-pass filtered potential temperature averaged over 30-120°E are shown for days indicated by numbers 4 and 5 in Fig.8 (Fig.9). The most notable feature is the downward expansion of the 350K isentropic surface between 10°N and 40°N. The hatched area in Fig.9 is proportional to the amount defined as $M_{350\text{-}360\text{K}} \equiv -g^{-1}(p_{360\text{K}} - p_{350\text{K}})$. where g is the gravity and p is pressure at the isentropic surface denoted by its suffix. It is easily understood that the value $M_{350\text{-}360\text{K}}$ indicates the air mass with its potential temperature between 350K and 360K within unit area.

It is shown that $M_{350\text{-}360\text{K}}$ is large on days indicated by ○ in Fig.8(b) and small on days indicated by × or △. As is indicated by the representative cross sections shown in Fig.9, the air mass between 350K and 360K expands and shrinks as the 200hPa potential temperature increases and decreases.

The time-pressure cross section for the 8-day low-pass filtered potential temperature averaged over 30-120°E and 20-40°N is shown in Fig.10. The symbols (○, × and △) and the numbers from 1 to 7 indicate the same dates as those in Fig.8. The increase and decrease of the $M_{350\text{-}360\text{K}}$ are evident, in accordance with the downward and upward displacements of the 350K isentropic contour.

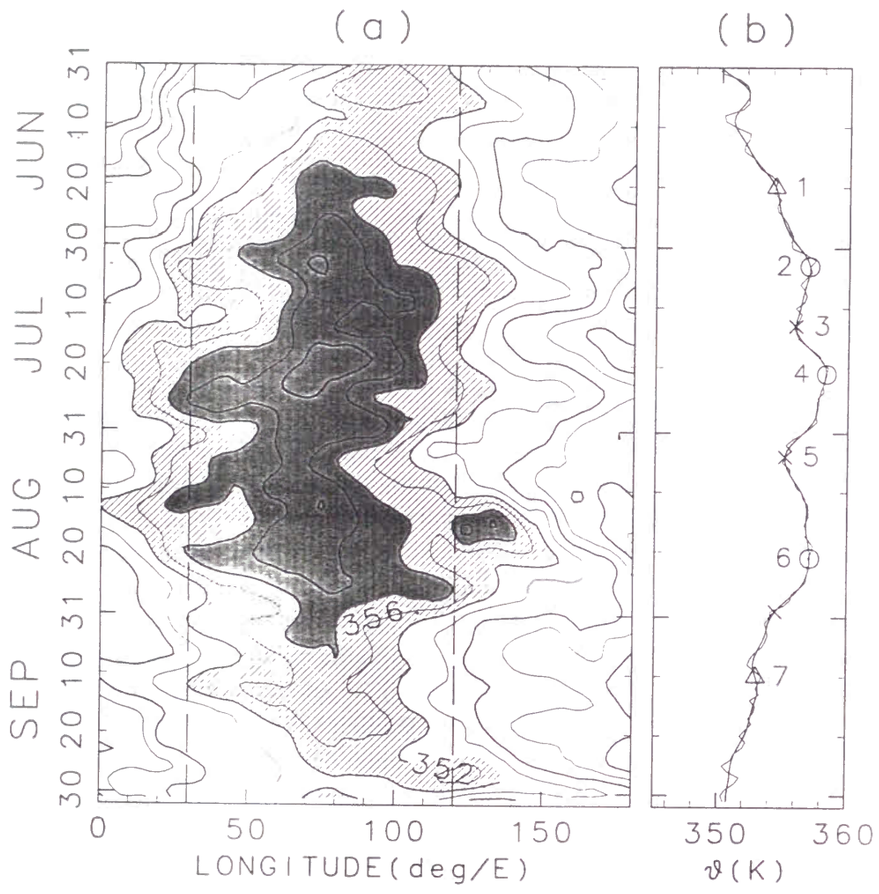

Fig. 8. (a)Longitude-time cross section along 20-40°N for 8-day low-pass filtered potential temperature at 200hPa, whose average over the region between two heavy dashed lines is shown in (b). Contour interval in (a) is 2K. Areas 352K $< \theta <$ 356K and 356K $< \theta$ are lightly and heavily hatched, respectively. The marks ○ and × indicate the major warming and cooling events, respectively. The mark △ shows the typical pre-onset and post-withdrawal days of the Indian summer monsoon. The numbers 1 to 7 are referred in the text.

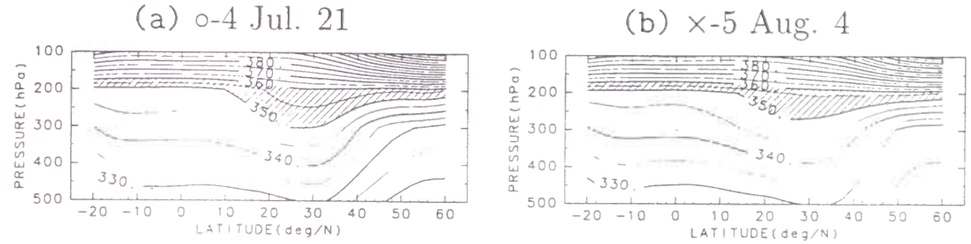

Fig. 9. The latitude-pressure cross sections of the potential temperature averaged over 30-120°E in 1983 on days indicated by the numbers 4 and 5 in Fig.8 are shown in (a) and (b), respectively. Contour interval is 5K. The areas of the 350-360K potential temperatures are hatched.

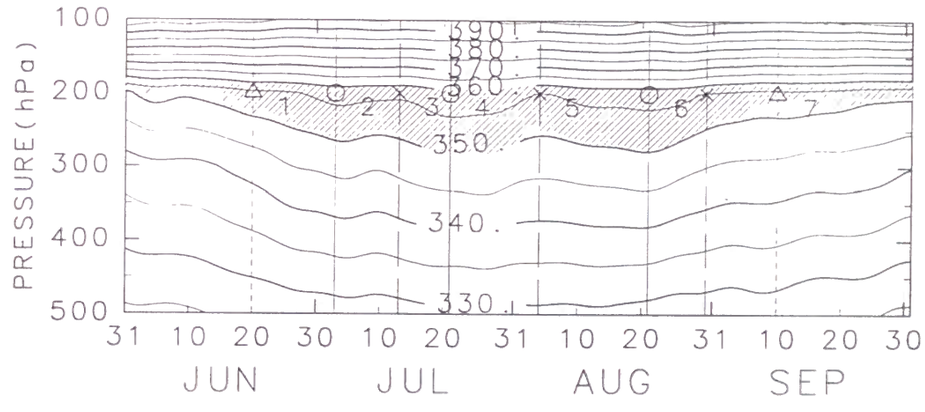

Fig. 10. The time-pressure cross section for potential temperature averaged over 30-120°E and 20-40°N in 1983. Contour interval is 5K. The area of 350-360K potential temperatures is hatched.

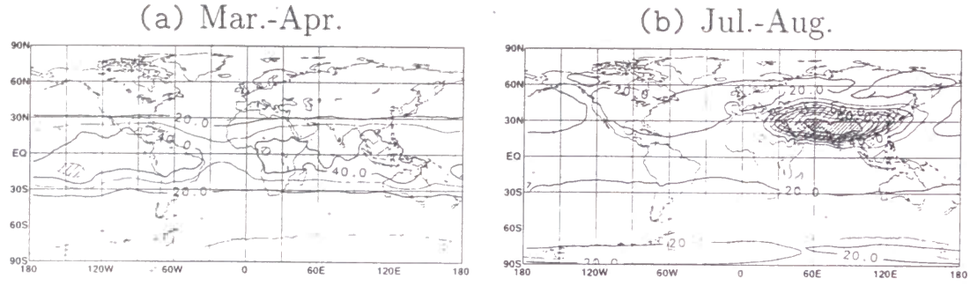

Fig. 11. The 2-monthly mean σ distributions on 355K isentropic surface. Contour interval is $10\text{kgm}^{-2}\text{K}^{-1}$. The areas greater than $50\text{kgm}^{-2}\text{K}^{-1}$ and $100\text{kgm}^{-2}\text{K}^{-1}$ are lightly and heavily hatched, respectively.

3.3 Mass transport on the isentropic surface in the northern periphery of the Tibetan Plateau in 1983

It is shown above that the warming and cooling in the upper troposphere over the Tibetan High region are related to the variations of $M_{350\text{-}360\text{K}}$. Here, new variable σ is introduced as follows:

$$\sigma = -g^{-1}\frac{\partial p}{\partial \theta}. \tag{1}$$

This variable indicates the amount of air mass within unit area and unit potential temperature increment. Around the 355K isentropic surface, σ is approximately proportional to $M_{350\text{-}360\text{K}}$.

Another distinctive character of σ is deduced from the mass continuity equation for the isentropic coordinates;

$$\frac{\partial}{\partial t}\sigma = -\nabla_\theta \cdot (\sigma \mathbf{v}) - \frac{\partial}{\partial \theta}(\sigma\dot{\theta}), \tag{2}$$

where $\mathbf{v}$ is the horizontal wind vector and $\dot{\theta}(= d\theta/dt)$ indicates the vertical velocity of the air parcel in the isentropic coordinate which corresponds to the diabatic effects. The differential operator ∇_θ represents the divergence of the vector field on the isentropic surface. If the air motion is adiabatic, the term including $\dot{\theta}$ vanishes and the local change of σ is caused only by the horizontal mass flux convergence on the isentropic surface. The diabatic effects cause the non-conservative mass 'production' or mass 'sink' on the isentropic surface.

The seasonal march of the 2-monthly mean $\sigma_{355\text{K}}$ distributions in 1983 are shown in Fig.11. Large $\sigma_{355\text{K}}$ is seen mainly from 30°S to 30°N in March-April. However, in July-August, extremely large $\sigma_{355\text{K}}$ extends over the region 10-150°E and 10-40°N. The maximum $\sigma_{355\text{K}}$ value reaches $100\text{kgm}^{-2}\text{K}^{-1}$, being confined in narrow region.

To assess how long the air mass is confined in the Tibetan High, the average time of an air parcel remaining is estimated from $\tau = \bar{\sigma}/\text{div}\overline{\sigma\mathbf{v}}$, where over bar denotes averaging over 1983

	terms	flux/$(10^9\text{kgK}^{-1}\text{s}^{-1})$ total	NB	SB	EB	WB
	$\delta\sigma/T$	-0.07				
	$\nabla_\theta \cdot (\bar{\sigma}\bar{\mathbf{v}})$	$+0.74$	$+0.27$	$+0.56$	$+0.37$	-0.46
	$\nabla_\theta \cdot (\overline{\tilde{\sigma}\tilde{\mathbf{v}}})$	$+0.14$	$+0.12$	-0.01	$+0.02$	$+0.01$
	$\nabla_\theta \cdot (\overline{\sigma'\mathbf{v}'})$	$+0.15$	$+0.16$	-0.02	$+0.01$	-0.00
$+)$	$\nabla_\theta \cdot (\overline{\tilde{\sigma}\mathbf{v}' + \sigma'\tilde{\mathbf{v}}})$	$+0.00$	$+0.01$	-0.00	$+0.00$	-0.00
	sum $(\bar{R})$	$+0.96$	$+0.56$	$+0.53$	$+0.40$	-0.45

Table 1. Amounts of each terms in (3) integrated over the domain 0-150°E and 20-40°N (the first column) and the contributions from respective boundaries; northern boundary NB, southern boundary SB, eastern boundary EB and western boundary WB (from the 2nd to 5th columns). They are calculated on 355K isentropic surface and averaged over July and August in 1983.

mid-summer (July and August) and the region including the almost whole of the Tibetan High. Though the values of τ vary more or less by the averaging region, they distribute near $\tau \simeq 30$days. For instance, in the region 30-120°E and 20-40°N, $\tau = 29$days. It means that the air parcels inserted in the 355K isentropic surface remain for about 30 days in the Tibetan High. The reason why the July-August $\sigma_{355\text{K}}$ is confined within such a relatively limited region should be related to the fact that continuous intense diabatic heating occurs in subtropical latitudes where the Coriolis parameter is large enough to maintain the large horizontal pressure gradient. Since this time scale may be sufficiently larger than that of the radiative cooling effect, evaluation of the radiative effect in these regions is also one of remaining important subjects for the estimation of the heating process on the intraseasonal or longer time scales quantitatively.

In order to research the processes which control $\sigma_{355\text{K}}$ in July and August, the $\sigma_{355\text{K}}$ budget is calculated here using the mass continuity equation for the isentropic coordinates, (2). Upon setting $\sigma = \bar{\sigma} + \tilde{\sigma} + \sigma'$ and $\mathbf{v} = \bar{\mathbf{v}} + \tilde{\mathbf{v}} + \mathbf{v}'$, σ and $\mathbf{v}$ represent the sum of the components of different time scales, where the over line denotes the average over the analysis period and $\tilde{\cdot}$ and $\cdot'$ denotes the variations on time scales which are longer and shorter than 15 days, respectively. By substituting this expression into (2) and averaging it over the analysis period, the following equation is obtained;

$$\frac{\delta\sigma}{T} = -\nabla_\theta \cdot (\bar{\sigma}\bar{\mathbf{v}}) - \nabla_\theta \cdot (\overline{\tilde{\sigma}\tilde{\mathbf{v}}}) - \nabla_\theta \cdot (\overline{\sigma'\mathbf{v}'}) - \nabla_\theta \cdot (\overline{\tilde{\sigma}\mathbf{v}' + \sigma'\tilde{\mathbf{v}}}) + \bar{R}. \tag{3}$$

where $\delta\sigma$ is the change of σ in the averaging period T, and $\bar{R}$ is the vertical flux divergence term, or the mass 'production' on this isentropic surface, which includes diabatic effects, mainly due to the intense convective clouds.

The budget analysis described above is applied for the period between July 1 and August 31 in 1983. The result averaged over 0-150°E and 20-40°N is tabulated in Table 1. It is shown that the diabatic effect $\bar{R}$ is mainly balanced with the divergence of σ flux by time mean flow, $\nabla_\theta \cdot (\bar{\sigma}\bar{\mathbf{v}})$, with the main outflow from the southern boundary. That on

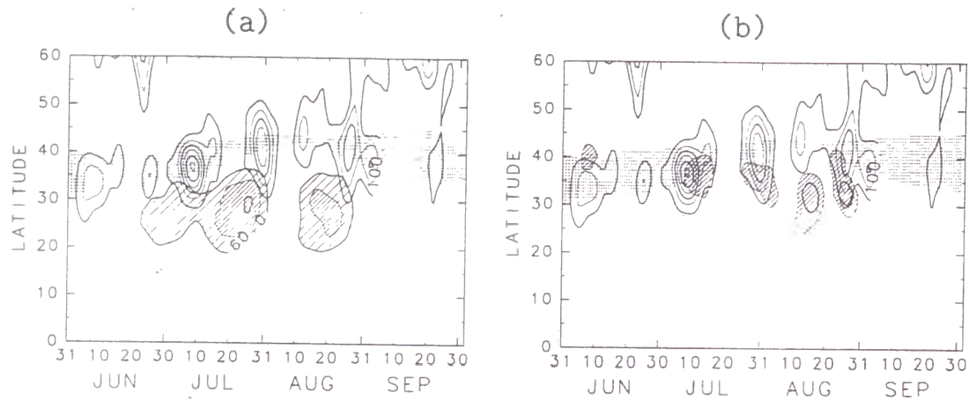

Fig. 12. Time-latitude cross sections for 60-day low-pass filtered u at 200hPa ($\bar{u}$), $\tilde{v}^2$ at 200hPa, and 8-day low-pass filtered σ and $\tilde{\sigma}\tilde{v}$ on 355K isentropic surface, averaged over 0-150°E. They are indicated by symbols $\bar{u}$, $\tilde{v}^2$, $\tilde{\sigma}$ and $\tilde{\sigma}\tilde{v}$, respectively in the figures. In (a), 8-day low-pass filtered σ is hatched. In (b), northward eddy σ-flux by intraseasonal disturbance on 355K isentropic surface ($\tilde{\sigma}\tilde{v}$) is indicated by hatched area. Contour intervals are $50\mathrm{m^2s^{-2}}$ for $\tilde{v}^2$, $15\mathrm{kgm^{-2}K^{-1}}$ for 8-day low-pass filtered σ, and $25\mathrm{kgm^{-1}s^{-1}K^{-1}}$ for $\tilde{\sigma}\tilde{v}$. Only significant contours are plotted. Areas where $\bar{u} > 25\mathrm{ms^{-1}}$ are shaded.

the northern boundary is also large but smaller compared to the southern boundary. The outflows by the intraseasonal ($\nabla_\theta \cdot (\overline{\tilde{\sigma}\tilde{\mathbf{v}}})$) and synoptic ($\nabla_\theta \cdot (\overline{\sigma'\mathbf{v}'})$) disturbance occur mainly on the northern boundary. Those on the southern boundary are significantly small. The northward eddy mass transport by the disturbances with intraseasonal time scales on the 355K isentropic surface is small compared to the total product of the air mass ($\bar{R}$) but not negligible compared to the northward mass flux in the northern periphery of the Tibetan High. The northward flux is especially large at 30-60°E (Figure is not shown here. See Fig.8 in Terao (1998b)).

In order to confirm further the role of the TQS-Rossby wave in northward transport of the air mass on the 355K isentropic surface, the relationships between the temporal variations of amplitude of the TQS-Rossby wave indicated by $\tilde{v}^2$ and, $\tilde{\sigma}_{355\mathrm{K}}$ and $\tilde{\sigma}_{355\mathrm{K}}\tilde{v}$ around the Tibetan High in 1983 are compared. Figure 12(a) shows the latitude-time cross sections averaged over 0-150°E for 60-day low-pass filtered u at 200hPa (shaded) which is referred by $\bar{u}$ hereafter, the 8-day low-pass filtered $\sigma_{355\mathrm{K}}$ (hatched) and $\tilde{v}^2$ at 200hPa. It is clearly shown that the $\sigma_{355\mathrm{K}}$ in the Tibetan High rapidly decreases when the intense TQS-Rossby wave is observed around July 9, July 30 and August 27 in the subtropical jet. In Fig.12(b), the northward σ-flux, $\tilde{\sigma}\tilde{v}$ at 355K (hatched), is superimposed upon $\bar{u}$ and $\tilde{v}^2$. The northward σ-flux is seen mainly at around 30-40°N. The variations in northward σ-flux are coincident with the TQS-Rossby wave amplifications in the subtropical jet. The large σ-flux well coincides

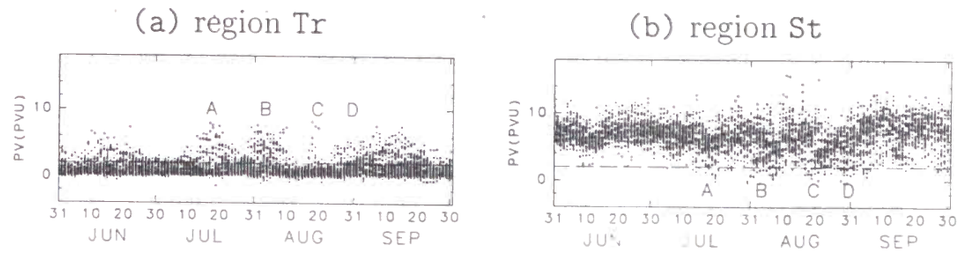

Fig. 13. Scatter diagrams showing the time change of distribution of PV at the 2.5° × 2.5° grid points at 00Z on each day for two typical areas (a)Tr (90-150°E and 15-25°N) and (b)St (150°E-150°W and 45-55°N) shown by boxes in Fig.11 of Terao (1998b). These areas are usually dominated by the tropospheric and stratospheric air, respectively. Horizontal dashed line shows 2PVU. Four marks A-D indicate the inferred active stratosphere-troposphere mass exchanging events.

with the decrease of σ except for the event at around August 15 when the hatched area in Fig.12(b) does not coincide with the TQS-Rossby wave.

These results suggest that the TQS-Rossby wave trapped in the subtropical jet regulates the mass budget on the 355K isentropic surface through the northward mass transport. In other words, some part of the warm air mass produced by the intense condensation heating is transported out of the Tibetan High when the TQS-Rossby wave is intensified in the subtropical jet producing the decrease in σ in the upper troposphere over the region near the Tibetan High.

3.4 Stratosphere-troposphere mass exchange on the 355K isentropic surface

In order to assess the stratosphere-troposphere (S/T) mass exchange around there, Ertel's potential vorticity, $PV = \sigma^{-1}(f + \zeta)$, is used, where f is Coriolis parameter and ζ is relative vorticity. This value PV can be used as a tracer of the air motion, since it is conserved in the isentropic flow. Besides, PV of stratospheric air is remarkably larger then that of tropospheric air. By using PV, the upper tropospheric air and the lower stratospheric air are distinguished from each other. In this study, the air with $PV < 2\mathrm{PVU}(10^{-6}\mathrm{kg^{-1}m^2s^{-1}K})$ is judged as the tropospheric air.

The PV distributions over the two regions indicated by boxes Tr (90-150°E and 15-25°N) and St (150°E-150°W and 45-55°N) (see Fig.11 of Terao (1998b)) are shown by scatter diagrams in Figs.13(a) and (b), respectively. The box Tr is usually dominated by the tropospheric air, while the box St is by the stratospheric air. However, in the box St, the tropospheric air mass are observed around the days indicated by A - D in Figs.13(a) and (b). On around the same days, in box Tr, the stratospheric air mass is observed. They should correspond to the S/T mass exchanging events.

name	U_e ms^{-1}	U_i ms^{-1}	K_e	K_i	ϕ	$b°$	Y	note
case-1	15.0	20.5	4.09	6.77	40°N	5	±35°	
case-2	12.6	18.1	5.11	7.32	37.5°N	5	±35°	Asian waveguide
case-3	14.1	18.0	4.87	5.88	45°N	5	±35°	Atlantic waveguide
case-4	24.7	34.5	5.23	7.35	25°S	5	±35°	Australian waveguide
case-5	21.3	22.4	3.09	3.50	52.5°S	5	±35°	S. H. Polar waveguide

Table 2. The list of the basic states used in this thesis. Parameters of U_e, U_i, K_e and K_i are defined in Appendix C.2. The assumed central latitude of the β-channel is noted by ϕ. The value b and Y are half width of westerly jet and the locations of the boundaries, respectively.

These events seem to occur at the same time or several days after the cooling events in Tibetan High (Fig.8) as far as three events indicated by A, B and D in Fig.13 are concerned. They also appear several days behind the energy peak of the TQS-Rossby wave activity (Fig.12).

4 The zonal wavelength and intensity of the TQS-Rossby waves reproduced in the β-channel model

In section 2, the systematic dependency of the zonal wavenumber and intensity on the frequency is found for the disturbance trapped in the subtropical jet over Eurasian Continent. In this section, the mechanism of this wavenumber-frequency dependency is explored using the simple zonally symmetric β-channel model. Afterward, the results of the model are compared to the data analysis using the space-time spectrum analysis.

4.1 The properties of the solutions of the step-like zonally symmetric basic state in the β-channel model

The step-like basic states in the β-channel model which is introduced in Appendix C.2 are solved. The variables and equations used in this subsection are defined in Appendix A to C. The ω-k relation of the solutions are related to **Q1** and **Q2** defined in section 1. The energy concentration ratio ϵ defined by (9) is useful in considering about **Q3**.

In Table 2, the cases examined in this thesis are listed. The basic state used in `case-1` (solid lines in Fig.14(a)) is derived from a sinusoidal basic state which is defined in Table 1 of Terao (1998c) (dashed lines in Fig.14(a)) using (10).

The dependency of c on k for all modes in `case-1` is plotted in Fig.14(b) with small circles (○). As is shown in Figs.3 and 4 of Terao (1998c), the spatial structure of 1-st mode solution is similar to the observed TQS-Rossby waves in the real atmosphere (e.g. Hsu and Lin (1992)).

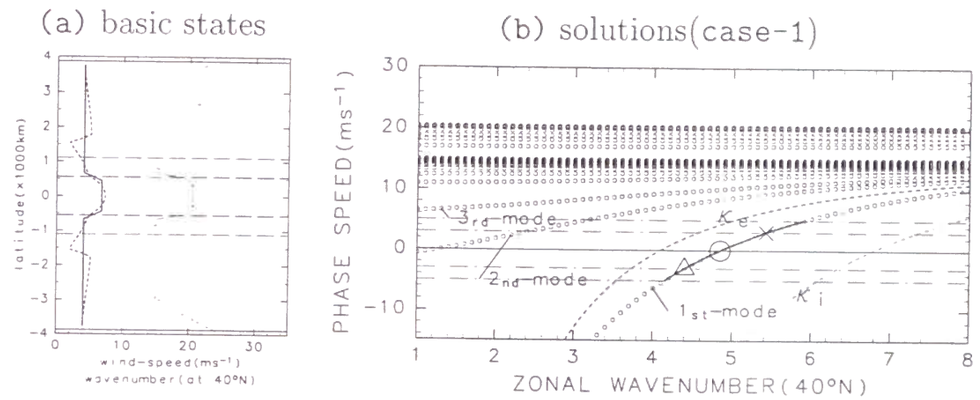

Fig. 14. (a)The meridional profiles of the basic states expressed by $U(y)$ (thin lines) and $K_s(y)$ (thick lines). The basic state used in `case-1` and the sinusoidal basic state from which the basic state of `case-1` is derived are shown by solid and dashed lines, respectively. Vertical and horizontal axes indicate the latitudinal location and unit of U and K_s in ms^{-1} and zonal wavenumber, respectively. Horizontal long dashed lines indicate the latitude $y = \pm 2b \approx \pm 1110$km and $y = \pm b \approx \pm 550$km. The thick horizontal lines at $y = \pm 7b \approx \pm 3870$km show locations of the boundaries. (b)The dependency of c on k of `case-1` solutions is represented by small circles (○). Horizontal long dot-dashed lines indicate $c = \pm 3$ms^{-1} and ± 5ms^{-1}. Marks ○, × and △ indicate solutions referred in the text. Thick solid line indicate the fraction of the solution curve which correspond to the TQS-Rossby wave trapped in the westerly jet (the TQS-Rossby wave solution curve fraction).

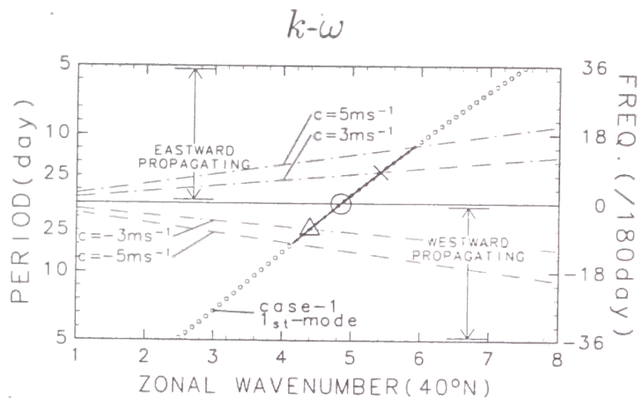

Fig. 15. Dependencies of ω on k variations of 1st-mode solutions for `case-1` (small open circles (○)). Thick lines show the TQS-Rossby wave solution curve fractions of `case-1`. The marks ×, △ and ○ indicate the locations of the solutions corresponding to those shown by the same marks in Fig.14(b). The dot-dashed lines indicate $c = \pm 3\text{ms}^{-1}$ and $\pm 5\text{ms}^{-1}$.

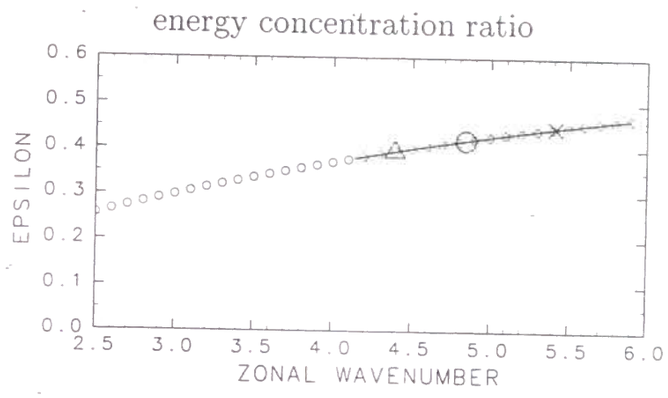

Fig. 16. The dependencies of ϵ on zonal wavenumber for the 1-st mode solutions of `case-1` (small open circles). The TQS-Rossby wave solution curve fraction is indicated by thick line. Marks ○, × and △ refer to the solutions indicated by the same marks in Figs.14(b).

To distinguish the trapped solutions, the values κ_r and κ_i (see (11)) are calculated and plotted in Fig.14(b) by thick and thin dotted lines, respectively. It is found that the solutions satisfying the condition (11) is found only on the 1-st mode solution curve. The solutions corresponding to the TQS-Rossby wave are on the fraction of 1-st mode solution curve, indicated by thick solid line in Fig.14(b). This fraction of solution curve which consists of the solutions corresponding to the TQS-Rossby wave is called the *TQS-Rossby wave solution curve fraction*, hereafter. Recall that the phase velocity of TQS-Rossby wave was defined to be between -5ms^{-1} and 5ms^{-1} in section 1.

The TQS-Rossby wave solution curve fraction is monotonically increasing function not only on this k-c plane (thick line in Fig.14(b)) but also on the k-ω plane (thick line in Fig.15). Therefore, if the frequency ω (or the zonal phase speed c) is given, the wavenumber k of solution is determined uniquely. The wavenumber of eastward- (westward-) propagating solution becomes large (small) as the absolute value of the frequency ($|\omega|$) increases.

In Fig.16, the distribution of energy concentration ratio ϵ defined by (9) for TQS-Rossby wave solution curve fraction of `case-1` is plotted by thick solid line. Generally speaking, ϵ of the eastward-propagating TQS-Rossby wave solution is greater than that of westward-propagating one.

4.2 Comparison between the solutions in the model and the observation

The space-time spectral densities (Hayashi, 1971) are calculated using the objective analysis data for four regions along the westerly jets in the northern hemisphere summer. The space-time spectral densities for both of streamfunction and meridional wind velocity are calculated, in order to examine the differences between them, for two selected regions. This should provide the sufficient informations to answer the **Q1** raised in 1. On the other hand, the availability of the step-like basic state in the β-channel model for the TQS-Rossby wave is assessed by investigating to what degree the space-time spectral peaks coincide with the k-ω dependencies of the TQS-Rossby wave solutions in the β-channel model and to what degree the intensities of the spectral peaks correspond to the calculated kinetic energy concentration ratio. They are related to the **Q2** and **Q3** raised in 1.

The space-time spectral densities are calculated for the westerly jet along the following four regions in northern summer;

Asian waveguide(`WG-1`): The subtropical westerly along 37.5°N over the Eurasian Continent and the western North Pacific from 0°E to 180°E.

Atlantic waveguide(`WG-2`): The subtropical westerly along 45°N over the eastern North Pacific, the American Continent and the Atlantic Ocean from 180°W to 0°W.

Australian waveguide(`WG-3`): The subtropical westerly in the southern hemisphere along 25°S over the Indian Ocean, Australian Continent and South Pacific from 60°E to 120°W.

Southern Hemispheric Polar waveguide(`WG-4`): The polar frontal jet along 52.5°S over the Antarctic Circumpolar Current from 60°E to 120°W.

They correspond to regions where the QS-Rossby waves are likely to be guided (see Fig.8 of Terao (1998c)). The space-time spectral densities along `WG-1`-`WG-4` are shown in Fig.17.

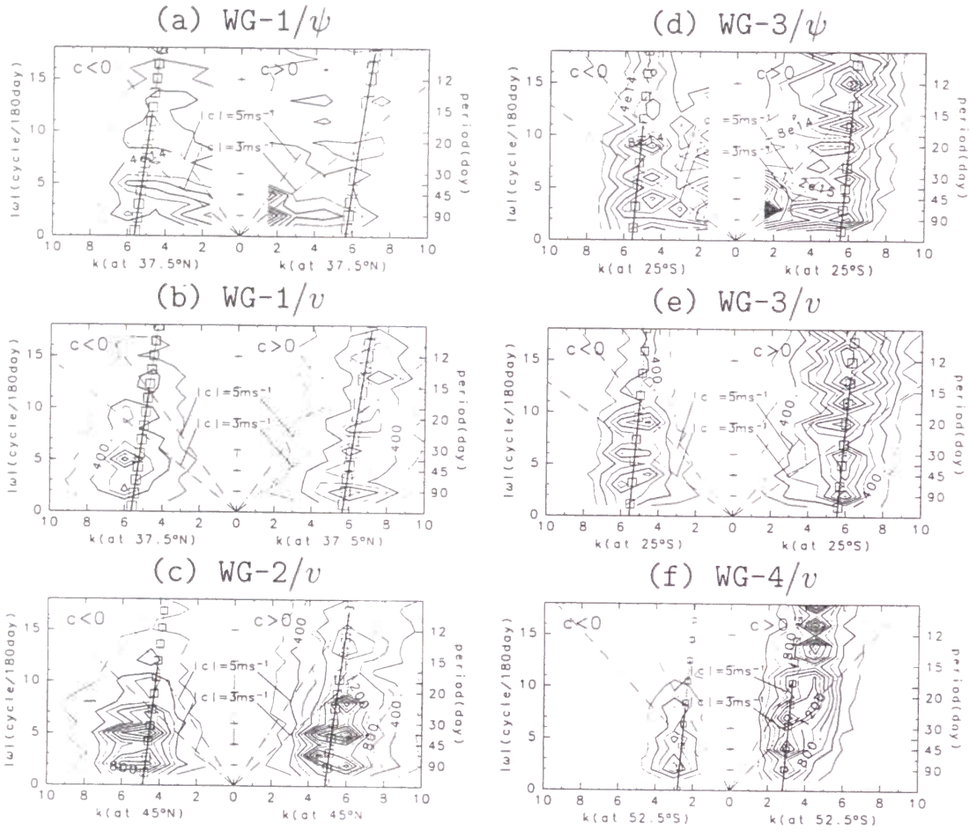

Fig. 17. The space-time spectral densities for 200hPa streamfunctions (a)along WG-1 and (d)along WG-3, and those for 200hPa meridional wind velocities along (b)WG-1, (c)WG-2, (e)WG-3 and (d)WG-4 are shown by contours. Contour intervals are $2.0\times10^{14}\mathrm{m}^4\mathrm{s}^{-2}$·deg·day and $2.0\times10^{2}\mathrm{m}^2\mathrm{s}^{-2}$·deg·day for the streamfunctions and the meridional wind velocities, respectively. Superimposed on them, the k-ω relationships for trapped solutions calculated for the basic states generated from the observed basic state near the corresponding jet are shown by the solid line with boxes (□). The thick parts of these lines show the TQS-Rossby wave solution curve fractions. The lengths of side of these boxes are proportional to the corresponding value of ϵ (see (9)). The dot-dashed lines indicate $c = \pm3\mathrm{ms}^{-1}$ and $\pm5\mathrm{ms}^{-1}$.

They are calculated using the FFT method for the longitude-time cross sections along the corresponding waveguides for 14 years from 1980 to 1993.

The space-time spectral densities of the streamfunctions and the meridional wind velocities are compared to each other for WG-1 and WG-3. While the spectral peaks become not so evident for the periods longer than 45 days for streamfunctions (Fig.17(a) and (d)), they remain evident for meridional wind velocities (Fig.17(b) and (e)). The spectral peaks for meridional wind velocities at about $k = 5.5$ exist for the periods up to 90 days. This implies that the TQS-Rossby waves are systematically seen not only in 10-30-day time scales but also up to 90-day time scales.

The k-ω relationships of the 1-st mode solutions of case-2-case-5 (see Table 2) are shown by the lines with boxes (□) in Fig.17. They are compared with the results of space-time spectrum analysis for the corresponding waveguides (the contour in Fig.17(a)-(f)).

As a whole, these figures show that the peaks in the space-time spectral densities are seen around the lines obtained from the TQS-Rossby wave solution curve fractions calculated from case-2-case-5. This indicates that the β-channel model well explains the observed zonal wavenumbers of the TQS-Rossby waves.

Furthermore, Fig.17 shows that the space-time spectral densities are large (small) where the magnitudes of ϵ's are large (small). This is consistent with the distribution of ϵ on the solution curve, which shows that ϵ's for eastward-propagating waves are generally larger than those of westward-propagating ones especially for larger frequency ranges.

5 Conclusions

In this thesis, the quasi-stationary Rossby wave trapped in the westerly jet (TQS-Rossby wave) are investigated from a viewpoint of the extratropical intraseasonal variations for the northern hemisphere summer.

Over the Eurasian Continent in summer, the TQS-Rossby wave-like disturbance is the most prominent factor of intraseasonal variations. The case study for the 1983 summer when the most representative TQS-Rossby wave-like disturbance is seen shows that a waveguide for the QS-Rossby wave is formed along the subtropical jet.

In the case study of 1983 summer, it is found that the TQS-Rossby wave on 30-45-day time scales plays an important role in regulating the intraseasonal variation of the Asian summer monsoon circulation and in the stratosphere-troposphere mass exchange. The mass budget analysis on the 355K isentropic surface averaged over July and August in 1983 shows that the northward eddy mass transport related to the TQS-Rossby wave plays an important role in the northward heat transport out of the Tibetan High. The temporal variation of the eddy heat transport, too, is fairly consistent with that of the TQS-Rossby wave as is summarized in Fig.18. Several days after the major warming events (H in Fig.18), the TQS-Rossby wave is amplified along the subtropical jet (R in Fig.18). At almost the same time, the northward mass transport on the 355K isentropic surface is found to be large (Fig.12(b)). The stratosphere-troposphere mass exchanging events are also observed just behind the northward mass transport (A, B and D in Fig.18). The structure of the TQS-

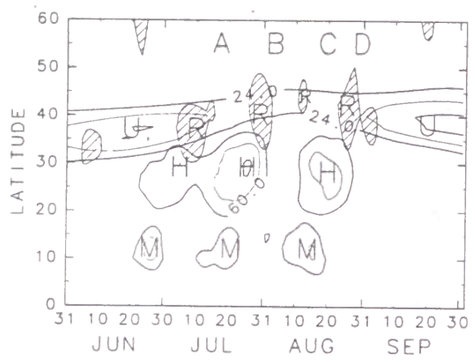

Fig. 18. Time-latitude cross section for 60-day low-pass filtered u at 200hPa (U), 8-day low-pass filtered σ at 355K (H), 8-day low-pass filtered u at 850hPa (M) and $\tilde{v}^2$ at 200hPa (R, hatched). The contour intervals are $4\mathrm{ms}^{-1}$. $15\mathrm{kgm}^{-2}\mathrm{K}^{-1}$ and $3\mathrm{ms}^{-1}$ for U, H and M, respectively. Contours smaller then $20\mathrm{ms}^{-1}$ for U, smaller than $45\mathrm{kgm}^{-2}\mathrm{K}^{-1}$ for H and smaller then $9\mathrm{ms}^{-1}$ for M are ignored. The areas where $\tilde{v}^2 > 150\mathrm{m}^2\mathrm{s}^{-2}$ are hatched. The marks A-D are the same dates as those shown in Fig.13.

Rossby wave along the subtropical jet also supports the above discussion suggesting strong interaction with the Tibetan High.

- The Tibetan High is strongly distorted when the TQS-Rossby wave passes.
- The critical latitude for the TQS-Rossby wave is just correspond to the center of the Tibetan High.
- The slight but systematic westward phase tilt of the TQS-Rossby wave supports the northward eddy heat flux.

These results support the discussion about the S/T exchange and its relation with the wave breaking (Dunkerton, 1995; Chen, 1995). In the literature, the effects of the intraseasonal variation of the Asian summer monsoon circulation on the extratropical circulations through the Rossby wave propagation are sought after (Kuma, 1985 and Yasunari, 1986). However, the results in this thesis show that the effects of the extratropical intraseasonal variation, i. e. the TQS-Rossby wave, on the Asian summer monsoon circulation through the wave breaking and the irreversible meridional mass exchange are important at least in 1983 summer.

By the space-time spectrum analysis using the data during 14 years (1980-1993), the dependencies on the frequency of the zonal wavenumber and the intensity of the TQS-Rossby wave are systematically described for the first time. Based on the results, the questions **Q1** to **Q3** can be answered as follows.

Answer to Q1: The TQS-Rossby waves are observed in rather wide frequency range not only on 10-30-day time scales but also up to 90-day time scale in the meridional wind velocity data. However the TQS-Rossby waves appear to be less evident compared to that by meridional wind in analysis using streamfunction (Figs.17(a) and (d)). It is dangerous to determine the predominant time scales of TQS-Rossby wave by the streamfunction or the geopotential height data only.

Answer to Q2: While the wavenumbers of the eastward and the westward-propagating modes of the TQS-Rossby wave are almost the same at lower frequency range, as the frequency increases, wavenumber of eastward- (westward-) propagating mode increases (decreases).

Answer to Q3: The intensity of westward-propagating mode becomes less evident than eastward-propagating one, as the frequency increases.

These observational facts are explained comprehensively by solving the β-channel model. The solution curve correspond to the TQS-Rossby wave is unique on the zonal wavenumber-frequency (k-ω) plane. The zonal wavenumber-frequency (k-ω) relation and the zonal wavenumber-trapping intensity (k-ϵ) relation are well coincide with the results of the space-time spectrum analysis for the TQS-Rossby waves.

The original analysis tools proposed are successfully used. The ray-path analysis for the Rossby wave (Hoskins and Ambrizzi, 1993; Yang and Hoskins, 1996) is extended. Not only temporally but also zonally appropriate smoothed basic flow is used instead of basic flows such as climatological or monthly mean flows smoothed only in time space. This method is available to the case study diagnosing the propagation route of the QS-Rossby wave packets.

The solutions of step-like zonally symmetric basic state is examined in the β-channel model, which clearly explains the dynamical aspect of the TQS-Rossby wave.

The intraseasonal variation of the Asian summer monsoon circulation is associated with the accumulation of the high potential temperature air mass transported into the upper troposphere around the Tibetan High. This accumulation is highly remarkable in the general circulations in the northern hemisphere summer. Investigating the accumulation, movement and releasing the air mass with high potential temperatures should be useful to study the mechanisms of the Asian summer monsoon circulation.

This thesis is based on the following articles:

- Barotropic Disturbances on Intraseasonal Time Scales Observed in the Midlatitudes over the Eurasian Continent during the Northern Summer
(北半球夏季にユーラシア大陸上の中緯度帯にみられる順圧的な季節内変動擾乱について)
Journal of the Meteorological Society of Japan, Volume 76 (1998), to be printed.

- The Relationships between Quasi-Stationary Rossby Waves in the Subtropical Jet And the Mass And Heat Transport in the Northern Periphery of the Tibetan High
(偏西風帯の準定常ロスビー波とチベット高気圧の北縁における質量・熱輸送との関係について)
Journal of the Meteorological Society of Japan, Volume 76 (1998), to be printed.

- The Zonal Wavelength of the Quasi-Staionary Rossby Wave Trapped in the Westerly Jet
(偏西風帯にトラップされる準定常ロスビー波の東西波長について)
Journal of the Meteorological Society of Japan, Volume 76 (1998), to be printed.

Acknowledgments

The author would like to thank Prof. Emeritus Hisafumi Muramatsu for constant encouragement and helpful suggestions on this research. He also thanks Prof. Hideji Kida and Mr. Noriyuki Nishi for their direction and valuable comments. The GFD-DENNOU Library is used for drawing many of the figures and numerical calculations. The data used are provided by the European Centre for Medium-Range Weather Forecasts(ECMWF). In order to solve the eigenvalues and eigenvectors of matrix, the LAPACK (Linear Algebra Package) subroutines are used.

Appendix

A The basic equations

The perturbation vorticity equation linearized about the zonally symmetric basic flow $U(y)$ in the β-plane is written in the following form,

$$\frac{\partial}{\partial t}\nabla^2\psi' + U\frac{\partial}{\partial x}\nabla^2\psi' + \beta_*\frac{\partial}{\partial x}\psi' = 0, \tag{4}$$

where ψ' is the perturbation streamfunction and β_* ($\equiv \beta - \frac{d^2U}{dy^2}$) is gradient of the absolute vorticity of the basic flow. Assuming that the perturbation with the zonal wavenumber $k(\geq 0)$ and the zonal phase speed c is in the form $\psi' \equiv \hat{\Psi}(y)e^{ik(x-ct)}$, the vorticity equation (4) reduces to the following second order ordinary differential equation;

$$(U-c)(\frac{d^2\hat{\Psi}}{dy^2} - k^2\hat{\Psi}) + UK_s^2\hat{\Psi} = 0, \tag{5}$$

where K_s is the *stationary total wavenumber* defined by

$$K_s^2 \equiv \frac{\beta_*}{U}. \tag{6}$$

This is the same as K_s defined in Hoskins and Ambrizzi (1993). Using c, the frequency of the disturbance can be written as $\omega = ck$.

If $c \neq U$, κ, the *Doppler shifted total wavenumber*, can be defined by

$$\kappa^2 \equiv \frac{U}{U-c}K_s^2, \tag{7}$$

which is equivalent to K defined in Yang and Hoskins (1996). Using this, (5) can be rewritten into the simpler form;

$$\frac{d^2\hat{\Psi}}{dy^2} = (k^2 - \kappa^2)\hat{\Psi}. \tag{8}$$

B The ray-path analysis for the QS-Rossby wave

B.1 The standard ray-path analysis

The ray-path theory to diagnose the behavior of the QS-Rossby wave used in this study is based on Hoskins and Ambrizzi (1993) and Yang and Hoskins (1996). The detailed explanations are made in section 5.1 in Terao (1998a). The coefficient κ defined above (7) is used to diagnose the behavior of the QS-Rossby wave on the basic flow U.

The propagation route of the QS-Rossby wave energy is diagnosed by the spatial distribution of κ as follows.

- When the QS-Rossby wavepacket with zonal wavenumber k propagating in the region where $\kappa > k$ reaches the *turning latitude* where $\kappa = k$, it turns to the κ-increasing direction. On the other hand, as the wavepacket approaches the *critical latitude* where $U = c$, it refracts toward the critical latitude and its meridional wavelength and meridional group velocity of the wavepacket tend to zero. The linear wave theory is invalid near such a latitude.

- When the QS-Rossby wave is trapped in the region with turning latitudes both northward and southward, it cannot escape from this region, i. e., it is guided. Such region is called *waveguide*.

B.2 An extension of the ray-path analysis — Representing certain spatial and temporal extensions of the wavepacket

The equation (7) shows that, the basic flow profile U is needed to derive κ. In the literature, the *climatological average* of observed u has been used for the basic flow profile. Recently, Naoe et al. (1997) examined the stationary Rossby wave propagations using the κ distributions derived from the *monthly mean* u's in winter as basic flows. However, since the patterns of κ obtained in their study are somewhat too complicated and involve smaller scale variations, it is difficult to interpret the patterns of κ.

Now, it should be reconsidered what the basic flow for the wavepacket is. Suppose a wavepacket propagating in the barotropic atmosphere. The behavior of the wavepacket at certain point is not determined only by u and $\frac{d^2u}{dy^2}$ at that point, but by the averaged basic flow in the area with certain temporal and zonal extent (hatched rectangular region in Fig.19). Therefore, the behavior of the wavepacket should be diagnosed using not only temporally but also zonally appropriately smoothed basic flow. More complete discussion about this extension is given in section 5.2 of Terao (1998a).

C The zonally symmetric β-channel model

C.1 Solving the model

Solving the disturbances in the β-channel model starts from (5). First, this differential equation is discretized about latitude y, where y is the meridional distance from the assumed central latitude of the β-channel. If the meridional profiles of $U(y)$ and $K_s(y)$ and the boundary conditions are provided, the possible structures of the disturbances and corresponding zonal phase velocities can be obtained for arbitrarily given k. If the area between two boundaries is discretized into $N+2$ grids at regular intervals including the boundaries, N pairs of the amplitude function $\hat{\Psi}_j(y)$ and the zonal phase speed c_j ($j = 1, \cdots, N$ and $c_1 \leq c_2 \leq \ldots \leq c_N$) are obtained. Here, the j-th solution is noted as *j-th mode solution*. The boundary conditions are set at two points $y = \pm Y$, where $\hat{\Psi} = 0$. This method is the same as those of Haltiner and Song (1962) and Yanai and Nitta (1968).

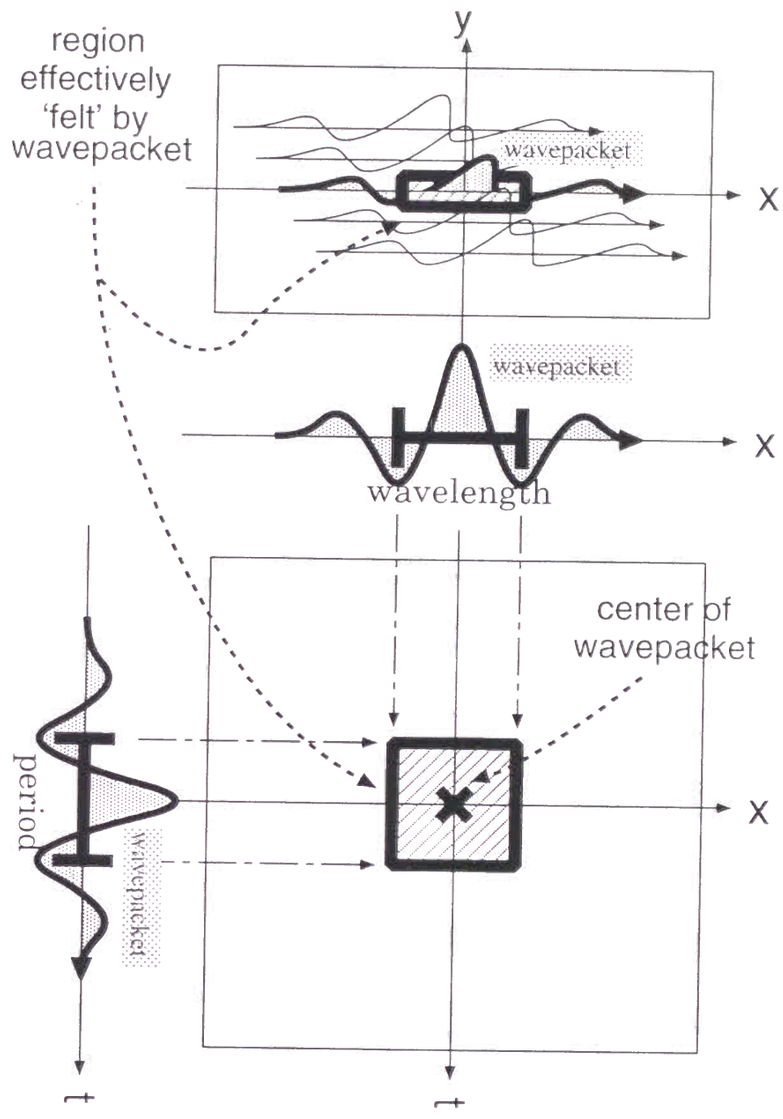

Fig. 19. A schematic diagram showing the temporal and spatial extent of the region which is effectively 'felt' by the wavepacket.

It should be noted that (5) has singularities at critical latitudes where $U = c$. Since only the solutions corresponding to QS-Rossby waves ($c < 5\text{ms}^{-1}$) are examined in this study, only those with slow zonal phase velocities are needed to be considered. In order for such solutions not to suffer the influence of the critical latitudes, the minimums of zonal flow ($U_{\min}$) of all the basic states used in this study are set larger than 10ms^{-1}.

As a measure which shows how strongly the solution is trapped in the westerly jet, the kinetic energy concentration ratio (ϵ) is introduced as follows:

$$\epsilon \equiv \frac{\int_{-b}^{b} \frac{1}{2}(\overline{u'^2 + v'^2})dy}{\int_{-Y}^{Y} \frac{1}{2}(\overline{u'^2 + v'^2})dy} \tag{9}$$

where b is the half-width of the westerly jet and u' and v' are the zonal and the meridional wind velocities of the perturbation.

C.2 The step-like basic states

The step-like basic states described below are used in the present study.

Two averaging operators, $\overline{(\cdot)}^{(i)}$ and $\overline{(\cdot)}^{(e)}$, are defined as the averaging over the domains $|y| \leq b$ (the internal domain) and $b \leq |y| \leq 2b$ (the external domain), respectively. From an original basic state, $U(y)$ and $K_s(y)$ which satisfy (6), the step-like basic state is generated by the following procedure.

$$\begin{cases} U(y) \equiv U_e \equiv \overline{U(y)}^{(e)} & \\ K_s^2(y) \equiv K_e^2 \equiv \overline{\beta_\star(y)}^{(e)} / \overline{U(y)}^{(e)} & (|y| > b) \\ U(y) \equiv U_i \equiv \overline{U(y)}^{(i)} & \\ K_s^2(y) \equiv K_i^2 \equiv \overline{\beta_\star(y)}^{(i)} / \overline{U(y)}^{(i)} & (|y| \leq b). \end{cases} \tag{10}$$

As the original basic state, any possible basic states such as the sinusoidal basic states or the basic states derived from the observational dataset can be used.

Now, it should be noted that this definition is somewhat tricky. Some supplementary explanations must follow. The equation (6) which indicates that the profile of K_s depends upon the profile of U prohibit us from determining the profile of K_s independent of U profile. However, if U and K_s are determined by (10), they no longer satisfy (6). Besides, to determine the profiles of K_s and U, only the original K_s and U profiles near the westerly jet ($-2b \leq y \leq 2b$) are used. The original profiles far from the westerly jet ($|y| > 2b$) are totally ignored. In spite of the tricky definition of the step-like basic state, however, the results obtained by the step-like basic states will be justified by the comparison of the results obtained from the sinusoidal and step-like basic states in section 2.4 of Terao (1998c). The reasons why the step-like basic state is justifiable are discussed in section 2.2.3 of Terao (1998c).

For step-like basic states, there is another distinct measure other than ϵ to distinguish the solutions which are trapped in the westerly jet. This measure is related to κ inside and outside the westerly jet noted by κ_i and κ_e, respectively. The equation (8) indicates

that the meridional structure of the solution at certain latitude becomes locally sinusoidal (exponential) if $k^2 - \kappa^2 < 0 (> 0)$. In order for the solution whose zonal phase speed is c to be trapped in the westerly jet, its zonal wavenumber k must satisfy

$$\kappa_e = K_e \sqrt{\frac{U}{U-c}} < k < \kappa_i = K_i \sqrt{\frac{U}{U-c}}, \tag{11}$$

since the wave must be sinusoidal inside the westerly jet and must decay exponentially outside. Consequently, utilizing the equation (11), values of κ_i and κ_e enable us to determine whether the solution with zonal wavenumber k and zonal phase speed c is trapped in the westerly jet or not.

References

Ambrizzi, T. and B. J. Hoskins, 1997: Stationary Rossby-wave propagation in a baroclinic atmosphere. *Quart. J. Roy. Met. Soc.*, **123**, 919–928.

Ambrizzi, T. , B. J. Hoskins, and H.-H. Hsu, 1995: Rossby wave propagation and teleconnection patterns in the austral winter. *J. Atmos. Sci.*, **52**, 3661–3672.

Blackmon, M. L. , Y.-H. Lee, and J. M. Wallace, 1984: Horizontal structure of 500mb height fluctuations with long, intermediate and short time scales. *J. Atmos. Sci.*, **41**, 961–979.

Blackmon, M. L. , Y.-H. Lee, and J. M. Wallace, 1984: Time variation of 500mb height fluctuations with long, intermediate and short time scales as deduced from lag-correlation statistics. *J. Atmos. Sci.*, **41**, 981–991.

Berbery, E. H. , J. Nogués-Paegle, and J. D. Horel, 1992: Wavelike southern hemisphere extratropical teleconnections. *J. Atmos. Sci.*, **49**, 155–177.

Chen, P. , 1995: Isentropic cross-tropopause mass exchange in the extratropics. *J. Geophys. Res.*, **100**, 16661–16673.

Duchon, C. E. , 1979: Lanczos filtering in one and two dimensions. *J. Appl. Meteor.*, **18**, 1016–1022.

Dunkerton, T. J. , 1995: Evidence of meridional motion in the summer lower stratosphere adjacent to monsoon regions. *J. Geophys. Res.*, **100**, 16675–16688.

Grose, W. L. and B. J. Hoskins, 1979: On the influence of orography on large-scale atmospheric flow. *J. Atmos. Sci.*, **36**, 223–234.

Hoskins, B. J. and T. Ambrizzi, 1993: Rossby wave propagation on a realistic longitudinally varying flow. *J. Atmos. Sci.*, **50**, 1661–1671.

Hayashi, Y. , 1971: A generalized method of resolving disturbances into progressive and retrogressive waves by space Fourier and time cross-spectral analyses. *J. Meteor. Soc. Japan*, **49**, 125–128.

Hsu, H.-H. and S.-H. Lin, 1992: Global teleconnections in the 250-mb streamfunction field during the northern hemisphere winter. *Mon. Wea. Rev.*, **120**, 1169–1190.

Haltiner, G. J. and R. T. Song, 1962: Dynamic instability in barotropic flow. *Tellus*, **14**, 383–393.

Johnson, R. H. , 1992: Heat and moisture sources and sinks of Asian monsoon precipitating systems. *J. Meteor. Soc. Japan*, **70**, 353–372.

Krishnamurti, T. N. and S. Gadgil, 1985: On the structure of the 30 to 50 day mode over the globe during FGGE. *Tellus*, **37A**, 336–354.

Kuma, K. , 1985: Linear response of the global atmosphere to thermal forcing during northern summer. *J. Meteor. Soc. Japan*, **63**, 739–747.

Knutson, T. R. and K. M. Weickmann, 1987: 30-60 day atmospheric oscillation: Composite life cycles of convection and circulation anomalies. *Mon. Wea. Rev.*, **85**, 1407–1436.

Kiladis, G. N. and K. M. Weickmann, 1992: Circulation anomalies associated with tropical convection during northern winter. *Mon. Wea. Rev.*, **120**, 1900–1923.

Lanzante, J. R. , 1990: The leading modes of 10-30 day variability in the extratropics of the northern hemisphere during the cold season. *J. Atmos. Sci.*, **47**, 2115–2140.

Lorenc, A. C. , 1984: The evolution of planetary-scale 200mb divergent flow during the FGGE year. *Quart. J. Roy. Met. Soc.*, **110**, 427–441.

Lau, K.-M. and T. J. Phillips, 1986: Coherent fluctuations of extratropical geopotential height and tropical convection in intraseasonal time scales. *J. Atmos. Sci.*, **43**, 1164–1181.

Madden, E. A. and P. R. Julian, 1971: Detection of a 40-50 day oscillation in the zonal wind in the tropical Pacific. *J. Atmos. Sci.*, **28**, 702–708.

Madden, E. A. and P. R. Julian, 1972: Description of global scale circulation cells in the tropics with a 40-50 day period. *J. Atmos. Sci.*, **29**, 1109–1123.

Madden, E. A. and P. R. Julina, 1994: Observations of the 40-50-day tropical oscillation — A review. *Mon. Wea. Rev.*, **122**, 814–837.

Murakami, M. , 1976: Analysis of summer monsoon fluctuations over India. *J. Meteor. Soc. Japan*, **54**, 15–31.

Nakamura, H. , 1994: Rotational evolution of potential vorticity associated with a strong blocking flow configuration over Europe. *Geophys. Res. Let.*, **43**, 2003–2006.

Nitta, T. , 1987: Convective activities in the tropical western Pacific and their impact on the Northern Hemisphere summer circulation. *J. Meteor. Soc. Japan*, **65**, 373–390.

Naoe, H. , Y. Matsuda, and H. Nakamura, 1997: Rossby wave propagation in idealized and realistic zonally varying flows. *J. Meteor. Soc. Japan*, **75**, 687–700.

Shapiro, L. J. and S. B. Goldenberg, 1993: Intraseasonal oscillations over the Atlantic. *J. Climate*, **6**, 677–699.

Simmons, A. J. , J. M. Wallace, and G. W. Branstator, 1983: Barotropic wave propagation and instability, and atmospheric teleconnection patterns. *J. Atmos. Sci.*, **40**, 1363–1392.

Terao, T. , 1995: Extratropical 20-30 day variations during the northern hemisphere summer. *Annuals of the Disaster Prevention Research Institute Kyoto University*, **38B-2**, 259–272(in Japanese).

Terao, T. , 1998a: Barotropic disturbances on intraseasonal time scales observed in the midlatitude over the Eurasian Continent during the northern summer. *J. Meteor. Soc. Japan*, **76**, (submitted).

Terao, T. , 1998b: The relationships between quasi-stationary Rossby waves in the subtropical jet and the mass and heat transport in the northern periphery of the Tibetan high. *J. Meteor. Soc. Japan*, **76**, (submitted).

Terao, T. , 1998c: The zonal wavelength of the quasi-staionary Rossby waves trapped in the westerly jet. *J. Meteor. Soc. Japan*, **76**, (submitted).

Tsuyuki, T. and K. Kurihara, 1989: Impact of convective activity in the western tropical Pacific on the East Asian summer circulation. *J. Meteor. Soc. Japan*, **67**, 231–247.

Yasunari, T. , 1979: Cloudiness fluctuations associated with the northern hemisphere summer monsoon. *J. Meteor. Soc. Japan*, **57**, 227–242.

Yasunari, T. , 1986: Low-frequency interactions between the summer monsoon and the northern hemisphere westerlies. *J. Meteor. Soc. Japan*, **64**, 693–708.

Yang, G.-Y. and B. J. Hoskins, 1996: Propagation of Rossby waves of nonzero frequency. *J. Atmos. Sci.*, **53**, 2365–2378.

Yanai, M. and T. Nitta, 1968: Finite difference approximations for the barotropic instability problem. *J. Meteor. Soc. Japan*, **46**, 389–403.